La radiologia medica (2021) 126:388–398
https://doi.org/10.1007/s11547-020-01298-5

CHEST RADIOLOGY

Third-generation iterative reconstruction on a dual-source, high-pitch, low-dose chest CT protocol with tin filter for spectral shaping at 100 kV: a study on a small series of COVID-19 patients

Andrea Agostini[1,2] · Alessandra Borgheresi[2] · Marina Carotti[1,2] · Letizia Ottaviani[2] · Myriam Badaloni[2] · Chiara Floridi[1,2] · Andrea Giovagnoni[1,2]

Received: 2 June 2020 / Accepted: 23 September 2020 / Published online: 12 October 2020

Abstract

Objectives To investigate the role of third-generation iterative reconstruction (ADMIRE) in dual-source, high-pitch chest CT protocol with spectral shaping at 100 kVp in Coronavirus disease 2019 (COVID-19).

Methods Confirmed COVID-19 inpatients undergoing to unenhanced chest CT were scanned with a dual-energy acquisition (DECT, 90/150Sn kV) and a dual-source, high-pitch acquisition with tin-filtered 100 kVp (LDCT). On the DECT with ADMIRE 3 (DECT3) were evaluated the pulmonary findings and their extension (25-point score). Two radiologists in consensus evaluated with 5-point scales the overall image quality, the anatomical structures, and the elementary findings on LDCT reconstructed with filtered backprojection (LDCT0), with ADMIRE 3 (LDCT3) and 5 (LDCT5), and on DECT3. The signal-to-noise ratio (SNR), the body mass index, the exposure times, and the radiation doses were recorded.

Results Seventy-five patients (57 M/18F; median age: 63 y.o.) were included, with median pulmonary extension of 13/25 points. The imaging findings were detected in proportion comparable to the available literature. The ADMIRE significantly improved the SNR in LDCT ($p < 0.00001$) with almost no significant differences in overweight patients. The LDCT had median effective dose of 0.39 mSv and acquisition time of 0.71 s with significantly less motion artifacts than DECT ($p < 0.00001$). The DECT3 and LDCT3 provided the best image quality and depiction of pulmonary anatomy and imaging findings, with significant differences among all the series ($p < 0.00001$).

Conclusion The LDCT with spectral shaping and ADMIRE3 provided acceptable image quality in the evaluation of patients with COVID-19, with significantly reduced radiation dose and motion artifacts.

Keywords X-ray computed tomography · Image reconstruction · Iterative reconstruction · CT protocol · Spectral shaping

Introduction

The pandemic spread of Coronavirus Disease 2019 (COVID-19) is representing an exceptional healthcare crisis with more than 23,000,000 confirmed cases, 815,000 deaths worldwide and significant impact on radiological facilities [1, 2].

In patients with COVID-19 and moderate or severe disease (e.g., signs of alveolar damage), chest imaging is recommended independently on the results or the availability of molecular tests [2]. Chest computed tomography (CT) is the most sensitive imaging tool for highlighting the imaging findings of COVID-19, for excluding potential differential diagnoses, and for the quantification of the pulmonary involvement [2].

The viral infection together with immune response leads to the pulmonary damage of COVID-19 detected on CT [3, 4]. The COVID-19 pneumonia has a complex, wide spectrum of CT manifestations: the most characteristic findings are the ground glass opacities (GGO), with or without consolidations, and main peripheral distribution [4]. However, the different CT patterns need to be recognized because

✉ Alessandra Borgheresi
alessandra.borgheresi@gmail.com

[1] Department of Clinical, Special and Dental Sciences, University Politecnica delle Marche, Ancona, Italy

[2] Department of Radiology, Division of Special and Pediatric Radiology, University Hospital "Umberto I – Lancisi – Salesi", Via Conca 71, 60126 Ancona, AN, Italy

their correlation with the evolution of the disease or their prognostic relevance [4–8].

Performing chest CT in mild-severe COVID-19 presents several issues. The accurate evaluation of CT findings requires high-quality images in the presence of motion artifacts (MA) related to dyspnea or cough [2, 6, 7]. On the other side, the potential concern about radiation exposure in patients undergoing serial examinations led some authors to suggest low-dose CT protocols [9, 10]. The management of MA in CT involves low rotation times and high pitch values, a particularly effective strategy on dual-source scanners (DSCT) [11]. Among the strategies for dose-reduction, the spectral shaping on the third-generation DSCT (Somatom Force, Siemens Healthineers, Erlangen) consists in a tin filter removing the low-energy component of the X-ray spectrum [12]; the higher photon efficiency provides images of good quality at reduced dose [13]. This technique can be associated with the Advanced Modeled Iterative Reconstruction (ADMIRE, Siemens Healthineers), a third-generation hybrid reconstruction algorithm with iterations in the raw-data domain (for statistical modeling and artifact reduction) and in the image domain (for noise reduction) [12].

Several studies evaluated the image quality of low-dose chest CT with spectral shaping [12–16] and demonstrated the beneficial role of Iterative Reconstructions (IR) [12, 14–16]. However, most of the studies in adults included tin-filter protocols with regular pitch values (< 2), while the high-pitch protocols with spectral shaping were evaluated mostly in pediatric populations with limited experience in adults [12–15, 17, 18]. Moreover, in most cases the image analysis was focused to nodular lesions in a regular pulmonary background (a so-called high-contrast recognition task) [12–15]. Conversely, evidences about the role of IR in low-contrast recognition tasks in thoracic imaging, such as the interstitial findings in COVID-19 pneumonia, are limited, with almost no systematic evaluation of IR [16]. The present study has two aims: (1) to report the CT findings in a population of COVID-19 patients undergoing to unenhanced chest CT; (2) to perform an objective and subjective analysis of image quality in order to optimize the use of ADMIRE for the evaluation of interstitial findings of a complex pulmonary disease with a low-dose, high-pitch acquisition with tin filter at 100 kV.

Materials and methods

Patient population

The present study, approved by the local institutional review board, is based on a retrospective review of prospectively included COVID-19 patients. Hospitalized patients > 18 years old, with COVID-19 infection confirmed at nasopharyngeal and oropharyngeal swab test, who underwent to baseline, unenhanced chest CT (in agreement with clinical needs) on the third-generation DSCT between March 10 and March 25, were included. The onset of respiratory symptoms was collected from patients' records. Patients' weight (W, [kg]) and height (H, [m]) were collected to calculate the body mass index (BMI) as $BMI = W/H^2$. Patients unable to raise the arms or the presence of medical implants, source of artifacts, were recorded. Patients undergoing to contrast-enhanced chest CT were excluded.

Image acquisition, reconstruction, and visualization

The CT protocol on the third-generation DSCT (Somatom Force, Siemens Healthineers, Erlangen) for symptomatic COVID-19 patients included a high-quality, dual-energy (DECT), helical acquisition and a sub-second, low-dose, high-pitch, dual-source acquisition (LDCT), all performed in end inspiration when possible, supine position, and caudo-cranial direction.

The DECT was set at 90/150Sn kV, with modulated mA (reference: 95 mAs), rotation time of 0.25 s, collimation of $2 \times 192 \times 0.6$ mm and a pitch of 1.05. The dual-source LDCT with spectral shaping (100 kV, 0.6 mm tin filter) had modulated mA (reference: 170 mAs), a rotation time of 0.25 s, a collimation of $2 \times 192 \times 0.6$ mm and a pitch of 2.5 (TurboFlash, Siemens Healthineers). Both the DECT and LDCT were reconstructed with a sharp kernel (Bl57) and a slice thickness/spacing of 1.5/1 mm. The DECT was reconstructed with ADMIRE at strength 3 (called DECT3) and a blending ratio of 0.7. For the comparative analysis and the evaluation of the role of ADMIRE in the low-dose protocol, the LDCT was reconstructed with filtered backprojection (FBP, called LDCT0) and with ADMIRE (strength 3 and 5, respectively LDCT3 and LDCT5) (Fig. 1).

All the images were anonymized and uploaded for comparative analysis on a dedicated workstation (Syngo.via VB20A, Siemens Healthineers).

Image evaluation: pulmonary findings

For descriptive statistics, two radiologists (with, respectively, 30 and 10 years of experience in thoracic radiology) evaluated in consensus on the DECT3 the imaging findings of COVID-19 in agreement with the definitions of the Fleischner Society and published case-series [4–8, 19]. The evaluated imaging findings were the different types of GGO, consolidations, reticular pattern, mixed pattern, subpleural lines, fibrous stripes, halo sign and reversed halo sign, air bronchogram, and subpleural sparing [4, 6, 7]. The airway changes included bronchiectasis and bronchial wall thickening [4, 6–8]. The presence of air bubbles, vascular enlargement (subsegmental vessels > 3 mm), nodules, sand-like

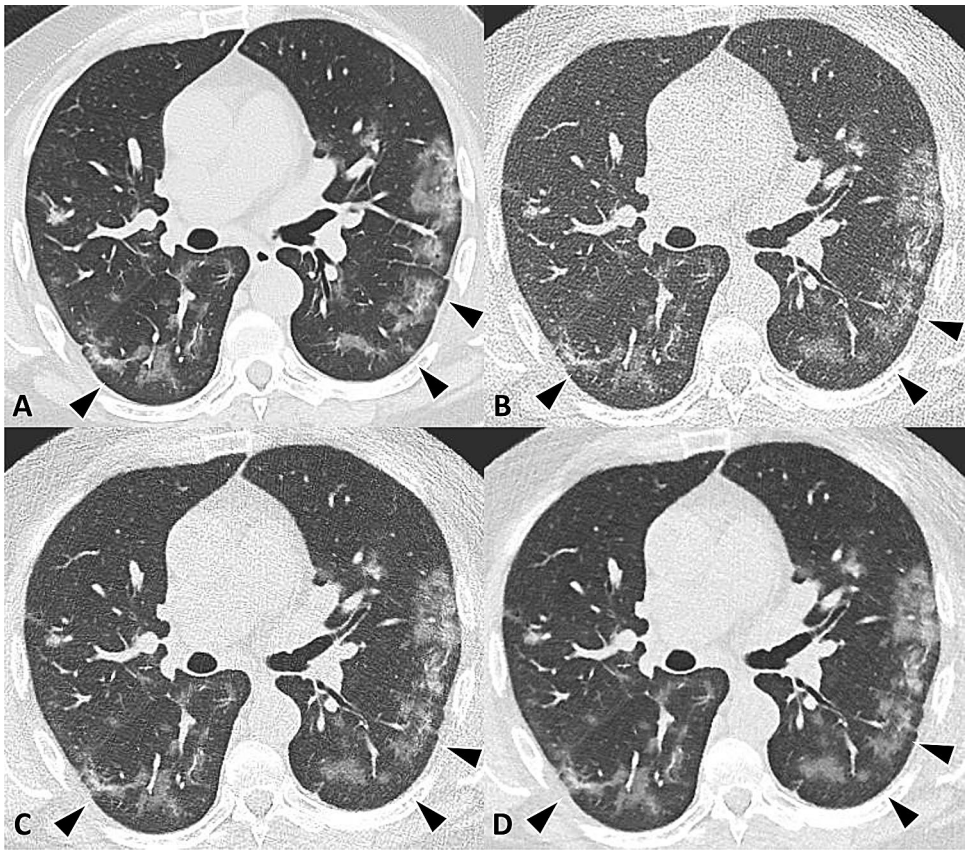

Fig. 1 Ground glass opacities with peripheral distribution and subpleural sparing (arrowheads) in a male patient, 58 y.o. with BMI of 27. **a** Dual-energy CT, 90/150Sn kV, ADMIRE 3. **b** High-pitch, dual-source acquisition with spectral shaping at 100 kV, filtered backprojection (LDCT0). **c** High-pitch, dual-source acquisition with spectral shaping at 100 kV, ADMIRE 3 (LDCT3). **d** High-pitch, dual-source acquisition with spectral shaping at 100 kV, ADMIRE 5 (LDCT5)

calcifications within consolidations, "tree-in-bud," and pleural changes (thickening or effusion) were evaluated [4–8]. Mediastinal lymphnodes and pericardial effusion were evaluated only for descriptive statistics [4]. The pulmonary findings were classified in central or peripheral (within the peripheral one-third of the lung). The extension of the pulmonary findings was also evaluated in consensus with a 25-point semi-quantitative score [6, 20]. The lobar extension of findings was visually scored as 0: no involvement; (1) $<5\%$; (2) 5–25%; (3) 26–49%; (4) 50–75%; (5) $\geq 75\%$. The 25-point score was the sum of the lobar scores.

Due to the complexity and the variety of the pulmonary findings, for subsequent analysis, the two radiologists grouped the patients in four predominant patterns, as described by Wang et al. [7]: GGO, consolidative, reticular, or mixed (Figs. 1, 2, 3).

Objective quality

A third radiologist (7 years of experience in thoracic radiology) placed circular regions of interest (ROI) at level of tracheal carina on pulmonary parenchyma, paraspinal muscle, subcutaneous fat, and tracheal air. Regions with major vessels or artifacts were avoided. The signal-to-noise ratio (SNR) was calculated as the fraction of the recorded mean attenuation (Hounsfield Units, HU) and standard deviation of each structure.

Subjective quality

To avoid the recognition bias, the subjective analysis was performed in consensus by the two radiologists in a separate session 1 month apart. Anonymized DECT3 (the reference standard) and LDCT were evaluated in casual order.

The subjective image quality included the following parameters: general quality (GQ), image sharpness (IS), and motion artifacts (MA), evaluated on 5-point scales. The scale for GQ and IS ranged from 1 (unacceptable) to 5 (excellent). The MA were evaluated from 1 (unacceptable) to 5 (absent); in scores 3–5, the MA had effect on depiction of pulmonary findings. The evaluated anatomical structures were fissures, central (up to segmental) or peripheral bronchovascular structures, and subpleural vessels (within 1 cm from the pleura).

The evaluation of different ADMIRE reconstructions required the definition of the so-called low-contrast recognition tasks for each predominant pattern, which were modeled by selecting three elementary findings for each predominant pattern, from a group of six elementary findings: GGO, septal thickening (interlobular or intralobular), architectural distortion, airway changes (bronchiectasis or bronchial wall

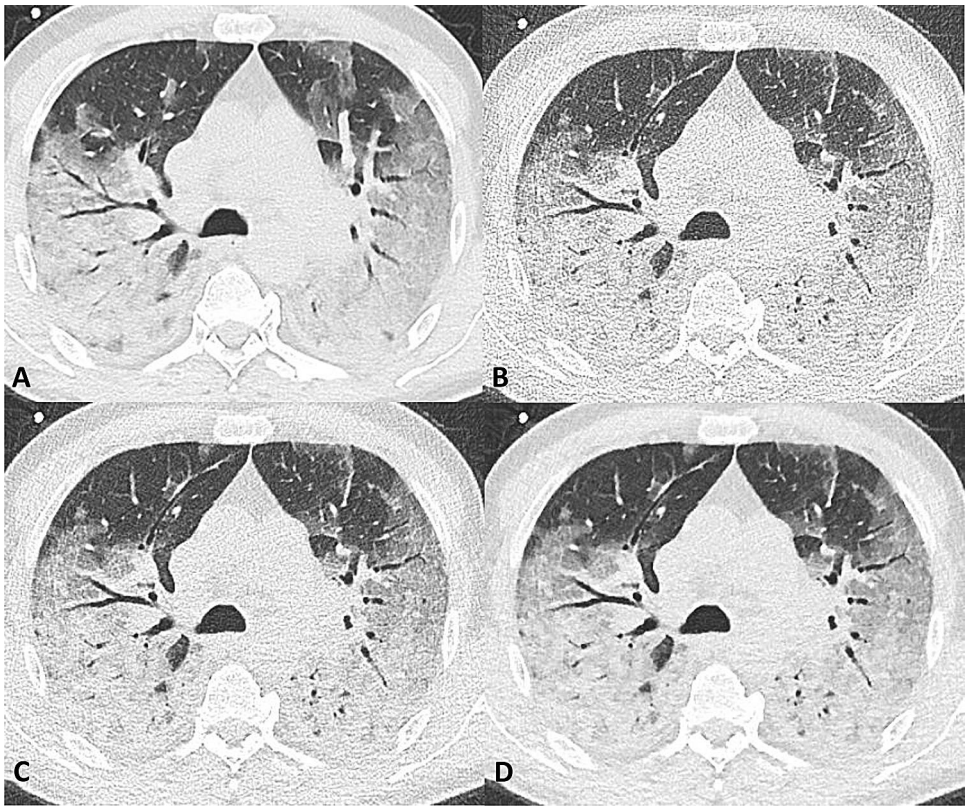

Fig. 2 Predominant consolidative pattern in a 67-year-old male patient with BMI of 26. Extended bilateral consolidations with air bronchograms and predominant posterior distribution. **a** Dual-energy CT, 90/150Sn kV, ADMIRE 3. **b** High-pitch, dual-source acquisition with spectral shaping at 100 kV, filtered backprojection (LDCT0). **c** High-pitch, dual-source acquisition with spectral shaping at 100 kV, ADMIRE 3 (LDCT3). **d** High-pitch, dual-source acquisition with spectral shaping at 100 kV, ADMIRE 5 (LDCT5). In A (DECT3) slight motion artifacts are present, not visible in B-D (LDCT)

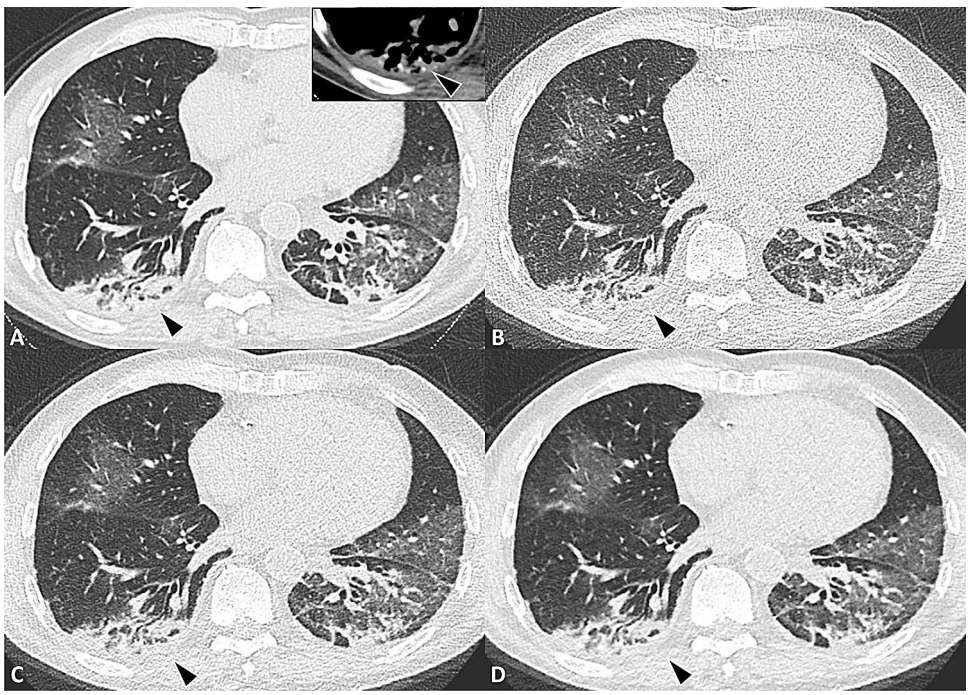

Fig. 3 Predominant mixed pattern in 78-year-old patient with BMI of 20. The mixed pattern (presence of consolidation, ground glass and reticular opacities in the presence of architectural distortion) is better depicted in the posterior, peripheral portions of lower lobes bilaterally. The arrowheads show a consolidation in the right lower lobe with contextual sand-like calcifications, better depicted in the image detail with mediastinal window in the upper right corner of **a**. **a** Dual-energy CT, 90/150Sn kV, ADMIRE 3. **b** High-pitch, dual-source acquisition with spectral shaping at 100 kV, filtered backprojection (LDCT0). **c** High-pitch, dual-source acquisition with spectral shaping at 100 kV, ADMIRE 3 (LDCT3). **d** High-pitch, dual-source acquisition with spectral shaping at 100 kV, ADMIRE 5 (LDCT5)

thickening), air bronchogram or air bubbles, and pleural changes (effusion or thickening).

Both the anatomical structures and pulmonary findings were evaluated with a 5-point scale: 1: unreliable depiction; 2–4 (severe, moderate, and slight blurring); 5: sharp delineation.

Radiation dose and exposure time

Exposure times and radiation dose (Computed Tomography Dose Index, CTDI [mGy], Dose Length Product, DLP [mGy * cm]) were recorded. The effective dose was calculated as ED = DLP × 0.014 [21].

Statistical analysis

All semiquantitative, categorical variables were expressed as frequencies and percentages. All numerical variables were tested for normality (Kolmogorov–Smirnov test). Since the numerical variables were not normal, they are expressed as median and interquartile ranges (25–75p). For objective analysis of SNR, patients were divided in BMI < 25 and BMI ≥ 25.

Nonparametric tests were used for numerical and categorical variables. In particular, the differences in extension of pulmonary findings across different lobes (Table 1), the differences in SNR (Table 2), the differences in semi-quantitative scales for image quality, anatomical structures, and elementary findings at different ADMIRE (Fig. 4, Table 3) were assessed with Friedman Test for multiple comparisons of related samples, and Conover post hoc analysis. The differences in SNR for patients with BMI < or ≥ 25 were assessed with Mann–Whitney test for unrelated samples (Table 2). The differences in exposure times and radiation doses in DECT and LDCT were assessed with Wilcoxon test for related samples. P values < 0.05 were considered significant. All calculations were performed with MedCalc v19.2.1 (MedCalc Software, Ostend, Belgium).

Results

Patient population and imaging findings

Seventy-five patients with confirmed COVID-19 were included (57 M/18F; median age: 63 years old; interquartile range: 54–72 years old). The median BMI was of 26 (IQR 25–29); 48 (64%) patients had a BMI ≥ 25. The CT scans were performed at a median of 8 days (interquartile range: 6–13) since the onset of symptoms. Seven (9%) patients were unable to raise the arms, 1 had a pacemaker, and 1 a metal implant on the right shoulder.

Table 1 shows the imaging findings evaluated on the DECT3 images: the most frequent were the GGO (74/75, 99%, Fig. 1), while consolidations were present in 55/75 (73%) of cases (Figs. 2, 3). The vascular enlargement and sand-like calcifications within consolidations (Fig. 3) were, respectively, detected in 63/75 (84%) and 9/75 (12%) of cases, while the sub-pleural sparing was recorded in 17 (23%) cases (Fig. 1). The most frequent distribution was in peripheral (40/75, 53%) (Figs. 1, 2, 3). The lower lobes were significantly more involved; the median CT score was of 13 of 25 (Table 1).

The mixed pattern was predominant in 28/75 patients (37%) (Fig. 3), followed by the predominant GGO pattern (27/75; 36%) (Fig. 1) and the predominant consolidative pattern (20/75; 27%) (Fig. 2). The reticular pattern was not predominant in any case.

Objective analysis

In Table 2, the SNR of all structures was significantly different in DECT3 and all LDCT with any ADMIRE. The SNR of tracheal air was significantly different in patients with BMI < 25 and ≥ 25 for any acquisition, while the SNR of pulmonary parenchyma was significantly different in patients with different BMI only in LDCT0 (Figs. 1, 2, 3).

Subjective analysis

Figure 4 summarizes the subjective evaluations of image quality and anatomical structures in DECT and LDCT for all 75 patients. All the parameters apart from motion artifacts had better scores in DECT3 than in LDCT; among LDCT, the LDCT3 achieved the best score.

Regarding the motion artifacts, the LDCT with any IR had significantly higher scores than DECT (Fig. 4). In particular, the motion artifacts in DECT 3 were scored as 1–3 (with marked influence on depiction of pulmonary findings) in 13 (17%) patients, and as 4–5 (minimal or no influence on depiction of pulmonary findings) in 62 patients. In LDCT, the motion artifacts were scored as 4–5 in all 75 patients (Figs. 2, 5).

In Table 3, the low-contrast recognition tasks for DECT and LDCT at different ADMIRE were assessed with the selected three elementary findings for each predominant pattern. The results showed in Table 3 agree with the trend depicted in Fig. 4: the elementary findings are better depicted in DECT3, while in LDCT, the best score is mostly achieved with ADMIRE at intermediate strength (LDCT3).

Radiation dose and exposure times

In Table 4, the LDCT protocol achieved significantly lower exposure times and radiation dose, respectively, lower than 1 s and 1 mSv.

Table 1 CT findings, distribution, predominant pattern and lung involvement in 75 patients with COVID-19 (DECT3)

CT findings	N (Total: 75)	%
GGO	74	99
Pure GGO	67	89
GGO and septal thickening	20	27
GGO with crazy paving	32	43
GGO with architectural distortion	59	79
Consolidation	55	73
Interlobular septal thickening	14	19
Mixed pattern	37	49
Honey combing	0	0
Subpleural lines	48	64
Fibrous stripes	48	64
Septal lines	29	39
Air bronchogram	31	41
Halo sign	6	8
Reversed halo sign	16	21
Bronchiolectasis	22	29
Bronchial wall thickening	50	67
Air bubble sign	26	35
Subpleural sparing	17	23
Vascular enlargement	63	84
Nodules	28	37
Sand-like classifications[a]	9	12
Tree in bud	2	3
Pleural thickening	42	56
Pleural effusion	9	12
Mediastinal lymph nodes	14	19
Pericardial effusion	11	15
Distribution		
Central	1	1
Peripheral	40	53
Both	34	45
Predominant pattern		
Ground glass opacity	27	36
Consolidation	20	27
Reticular pattern	0	0
Mixed pattern	28	37
Involvement, CT score	Median (25–75p)	N (%)
LUL	3 (2–3)*	72 (96)
LLL	3 (2–4)*	73 (97)
RUL	2 (1–3)*	69 (92)
RML	1 (1–3)*	65 (87)
RLL	3 (2–4)*	73 (97)
Total CT score	13 (9–17)	

LUL Left upper lobe, *LLL* left lower lobe, *RUL* right upper lobe, *RML* right middle lobe, *RLL* right lower lobe, *GGO ground glass opacities*, 25–75p: interquartile range

*Friedman test, $p < 0.00001$. Post hoc analysis: the lower lobes were significantly more involved than the upper lobes and the middle lobe

[a]Within consolidations

Table 2 Objective image quality: signal-to-noise ratio (SNR)

SNR	BMI	DECT3 Median (25–75p)	LDCT0 Median (25–75p)	LDCT3 Median (25–75p)	LDCT5 Median (25–75p)	p*
Tracheal air	< 25 ($N = 27$)	34.61 (29.57–41.41)	8.40 (7.21–10.06)	15.45 (13.50–17.79)	28.56 (26.60–33.07)	< 0.00001
	≥ 25 ($N = 48$)	30.36 (26.72–36.56)	7.23 (6.20–8.51)	12.91 (11.36–15.28)	24.53 (22.14–29.00)	< 0.00001
	p[a]	0.0341	0.0014	0.0007	0.0055	
Lung parenchyma	< 25	15.79 (12.89–25.06)	6.38 (5.50–7.66)	10.53 (8.51–11.56)	16.82 (11.62–18.43)	< 0.00001
	≥ 25	16.94 (14.60–18.43)	5.64 (4.84–6.64)	9.35 (7.89–10.91)	15.88 (13.30–18.13)	< 0.00001
	p[a]	0.6668	0.0406	0.1890	0.8039	
Paraspinal muscle	< 25	0.96 (0.76–1.04)	0.24 (0.20–0.28)	0.39 (0.34–0.50)	0.82 (0.59–0.96)	< 0.00001
	≥ 25	0.85 (0.68–1.03)	0.22 (0.20–0.26)	0.365 (0.31–0.45)	0.69 (0.60–0.85)	< 0.00001
	p[a]	0.1945	0.2258	0.0790	0.3395	
Subcutaneous fat	< 25	2.02 (1.70–2.34)	0.45 (0.34–0.50)	0.75 (0.63–0.88)	1.44 (1.27–1.60)	< 0.00001
	≥ 25	1.86 (1.65–2.37)	0.42 (0.37–0.47)	0.73 (0.61–0.84)	1.47 (1.26–1.70)	< 0.00001
	p[a]	0.6628	0.5180	0.4865	0.7488	

DECT3 Dual-energy CT, ADMIRE 3, *LDCT* low-dose CT with spectral shaping, filtered backprojection, *LDCT3* LDCT with ADMIRE 3, *LDCT5* LDCT with ADMIRE5, *25–75p* interquartile range, *SNR* signal-to-noise ratio, *BMI* body mass index

*Friedman test. Post hoc analysis: significant differences between DECT3, LDCT0, LDCT3, LDCT5 in pairwise comparisons

[a]Mann–Whitney test

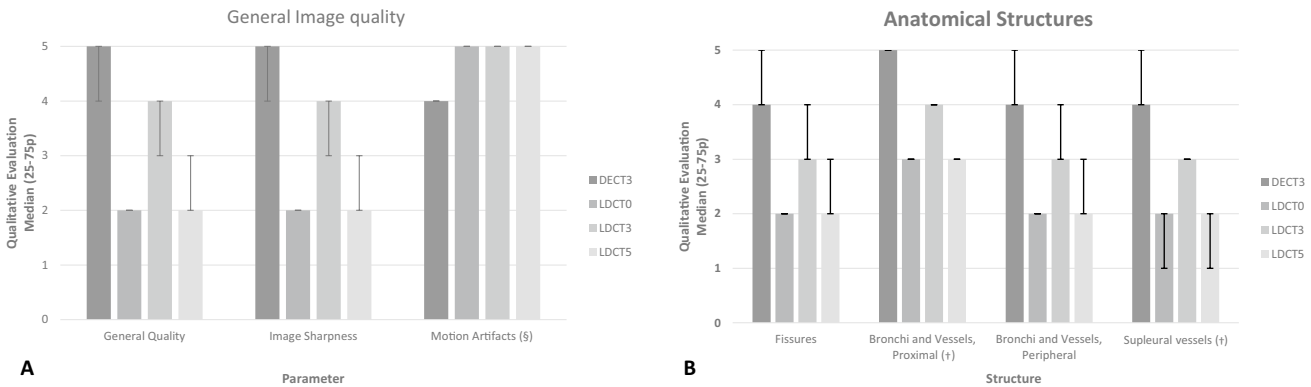

Fig. 4 Bar Graph showing the subjective image analysis on 5-point scales (see text). The bars show the median score for each parameter, series, and iterative reconstruction. The error bars show the interquartile range (25–75p). **a** Overall image quality including the general quality, image sharpness, and motion artifacts. **b** Anatomical structures including pleural fissures, proximal bronchi and vessels (up to segmental), peripheral bronchi and vessels, and subpleural vessels (within 1 cm from pleura). Significant differences among the semiquantitative scores for all parameters, series and reconstruction were recorded (Friedman, $p < 0.00001$). Post hoc analysis: (§): significant differences between DECT3 and LDCT at any ADMIRE; differences among LDCT were not significant. (†): differences between LDCT5 and LDCT0 were not significant. In all other cases, significant differences were found between DECT3, LDCT0, LDCT3, LDCT5 in pairwise comparison. DECT3: Dual-energy CT, ADMIRE 3. LDCT0: Low-dose CT with spectral shaping, Filtered Backprojection. LDCT3: Low-dose CT with spectral shaping, ADMIRE 3. LDCT5. Low-dose CT with spectral shaping, ADMIRE 5

Table 3 Subjective image analysis in different predominant patterns

	N (Tot. 75)	DECT3 Median (25–75p)	LDCT0 Median (25–75p)	LDCT3 Median (25–75p)	LDCT5 Median (25–75p)	*p**
Predominant pattern: GGO (N = 27)						
GGO	27	5 (5–5)	2 (2–2)	4 (4–4)	3 (2–3)	< 0.00001
Septal thickening[a]	25	5 (4–5)	2 (1–2)	3 (3–4)	2 (1–2)	< 0.00001[§]
Airway changes[b]	15	5 (5–5)	2 (2–2)	4 (4–4)	2 (2–3)	< 0.00001[§]
Predominant pattern: consolidation (N = 20)						
Air Bronchogram or air bubbles	17	4 (4–5)	2 (2–2)	3 (3–3)	2 (2–3)	< 0.00001
Airway changes[b]	14	4 (4–5)	2 (2–3)	3 (3–4)	2 (1–3)	< 0.00001[§]
Pleural changes[c]	11	4 (4–4)	2 (2–2)	3 (3–3)	3 (2–3)	< 0.00001[†]
Predominant pattern: mixed (N = 28)						
GGO	28	5 (4–5)	2 (2–2)	4 (3–4)	3 (2–3)	< 0.00001
Air bronchogram or air bubbles	17	5 (4–5)	2 (2–2)	4 (3–4)	3 (2–3)	< 0.00001
Architectural distortion	26	5 (4–5)	2 (2–3)	4 (3–4)	3 (2–3)	< 0.00001

DECT3 Dual-energy CT, ADMIRE 3. *LDCT* low-dose CT with spectral shaping, Filtered Backprojection, *LDCT3* LDCT with ADMIRE 3. *LDCT5* LDCT with ADMIRE 5, *25–75p* interquartile range, *GGO* ground glass opacities

*Friedman test. Post hoc analysis. [§]Differences between LDCT5 and LDCT0 were not significant. [†]Differences between LDCT3 and LDCT5 were not significant. In all other cases, significant differences were found between DECT3, LDCT0, LDCT3, LDCT5 in pairwise comparison

[a]Interlobular or intralobular (crazy paving)

[b]Bronchiectasis or bronchial wall thickening

[c]Pleural thickening or pleural effusion

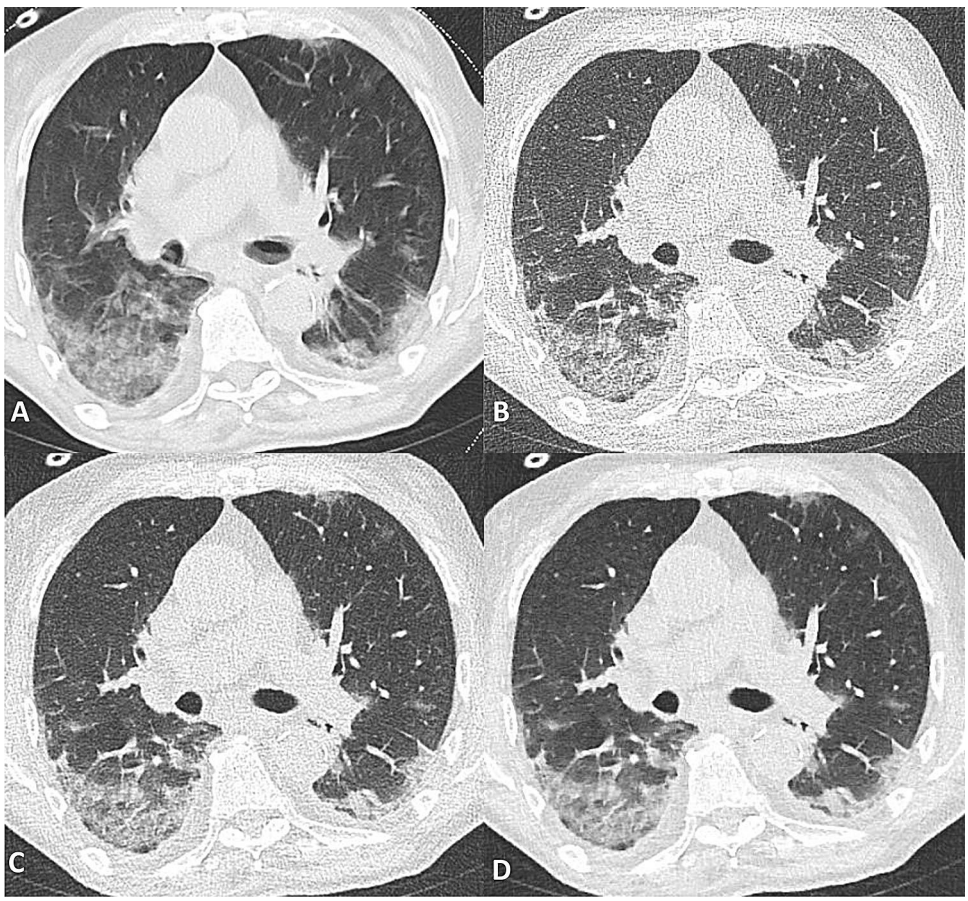

Fig. 5 Motion Artifacts in a male patient, 79 y.o. with BMI of 18. **a** Dual-energy CT, 90/150Sn kV, ADMIRE 3. **b** High-pitch, dual-source acquisition with spectral shaping at 100 kV, filtered backprojection (LDCT0). **c** High-pitch, dual-source acquisition with spectral shaping at 100 kV, ADMIRE 3 (LDCT3). **d** High-pitch, dual-source acquisition with spectral shaping at 100 kV, ADMIRE 5 (LDCT5). The motion artifacts in **a** (DECT3, coughing patient) significantly affect the depiction of interstitial thickening within the ground glass opacities and the subpleural sparing in the lower lobes. The LDCT are free of motion artifacts; the interstitial thickening is better depicted when the ADMIRE is used (**c**, **d**). Pleural thickening is also present

Table 4 Exposure times and radiation dose

	DECT3 Median (25–75p)	LDCT Median (25–75p)	p^a
Exposure time	2.07 (1.97–2.15)	0.71 (0.64–0.75)	< 0.0001
CTDI (mGy)	6.81 (6.24–9.11)	0.73 (0.65–0.81)	< 0.0001
DLP (mGy * cm)	306.66 (250.11–380.95)	26.82 (24.12–29.85)	< 0.0001
ED (mSv)	4.45 (3.63–5.52)	0.39 (0.35–0.43)	< 0.0001

DECT3 Dual-energy CT, ADMIRE 3, *LDCT* Low-dose CT with spectral shaping, *25–75p* interquartile range, *CTDI* computed tomography dose index, *DLP* dose length product, *ED* effective dose

[a]Wilcoxon test

Discussion

The present work highlights the role of ADMIRE applied to a high-pitch, dual-source acquisition with spectral shaping at 100 kV in 75 hospitalized patients with mild-severe pulmonary involvement by COVID-19 (median CT score: 13 of 25, Table 1). The different patterns of COVID-19 pneumonia were chosen as model to evaluate the role of ADMIRE in the so-called low-contrast recognition tasks in the high-pitch, dual-source CT protocol [4].

The imaging findings were reported in a proportion comparable to the already published data, the most peculiar being the GGO, consolidations, and the vascular enlargement [4–8]. The proportion of subpleural sparing was comparable to what reported in Tabatabaei et al. [8] (Fig. 1). Unlike other case-series, we noticed sand-like calcifications within consolidations in 12.0% of cases (Fig. 3). The sand-like calcifications were anecdotally assessed in few case-series and could be eventually considered an uncommon finding of COVID-19 [22, 23]. Calcifications have been related to several non-infectious and infectious diseases, including granulomatous, fungal, parasitic, and viral pneumonias [19, 24]. As an example, alveolar pulmonary calcifications have been described after the recovery of Varicella pneumonias [25]. The eventual correlation between sand-like calcifications and COVID-19 pneumonia, as well as the diagnostic and prognostic relevance, needs to be further investigated.

The CT protocol for COVID-19 included a high-quality DECT with a relatively short acquisition time and the possibility of post-processing in case of artifacts (11% of patients were unable to maintain the arms raised or had implanted devices) [26]; the selected ADMIRE 3 already demonstrated optimal image quality [13, 16]. In our population, MA were present in a discreet proportion of cases and significantly affected the depiction of CT findings in 17% of patients (Fig. 5), hence, the CT protocol included a high-pitch, dual-source scan. The LDCT had a pitch value of 2.5 to achieve adequate dual-source sampling with a scan Field-Of-View (sFOV) of 400 mm in a sub-second acquisition. Thus, the LDCT allowed for adequate control of MA with only minimal effect on depiction of imaging findings (Figs. 2, 5), while the spectral shaping achieved an ED < 1 mSv (median: 0.38 mSv), the same order of magnitude of a double-projection chest X-ray (Table 4) [9, 21].

As expected, the ADMIRE at increasing strengths significantly improved the SNR of LDCT acquisitions (Table 2); moreover, the ADMIRE decreases or avoided differences in SNR (except for the tracheal air) between overweight patients and patients with normal BMI. These data agree with the published literature (Table 2, Figs. 1, 2, 3) [12, 15, 16, 27–29].

Three predominant patterns were recognized in our patients; the evaluated elementary findings were chosen because of their relevance (e.g., prognostic) and to simulate a so-called low-contrast detection task (e.g., the septal thickening superimposed to GGO; Table 3, Fig. 6) [30]. In all the three scenarios, we recorded the same trend as the qualitative analysis, where the ADMIRE improved the image quality and depiction of findings, but higher levels of ADMIRE did not improve the median scores, confirming the ADMIRE 3 as acceptable (Table 3, Fig. 4) [13, 16].

A technical challenge in the implementation of IR is the distinction of edges in low-contrast objects and background noise, in particular at lower radiation doses and higher strength of IR [30]. This problem has already been evaluated in liver imaging. Baker et al. found a significantly higher image quality but degraded detection of low-contrast liver lesions at lower doses and higher strength of IR (SAFIRE, Siemens Healthineers) [27]. Jensen et al. confirmed a lower detection rate of small colorectal liver metastases in low-dose protocols and different IR (ASIR and ASIR-V, GE Healthcare) [28].

In thoracic imaging, the performance of IR and spectral shaping and IR has been evaluated mostly in high-contrast recognition tasks. Gordic et al. [12] found better image quality and higher sensitivity and diagnostic confidence for lung nodule detection on phantoms with spectral shaping at 100 kV and ADMIRE 5. Martini et al. [14] confirmed a higher sensitivity for nodule detection on phantoms at increasing level of ADMIRE; for subsolid nodules, the ADMIRE 5 had a sensitivity comparable or lower to ADMIRE 3 in lowest dose acquisitions. Moreover, Martini et al. [15] found improved image quality and nodule detection in humans with ADMIRE 5; however, with ADMIRE5 the authors found lower agreement rates in detection of interstitial changes and emphysema compared to the ADMIRE 3, being the standard-dose acquisition the reference.

Our results confirm the feasibility of low-dose chest CT acquisition with spectral shaping, and the fundamental role of ADMIRE to achieve an acceptable image quality [12–16]. However, at increasing level of ADMIRE, the low-contrast

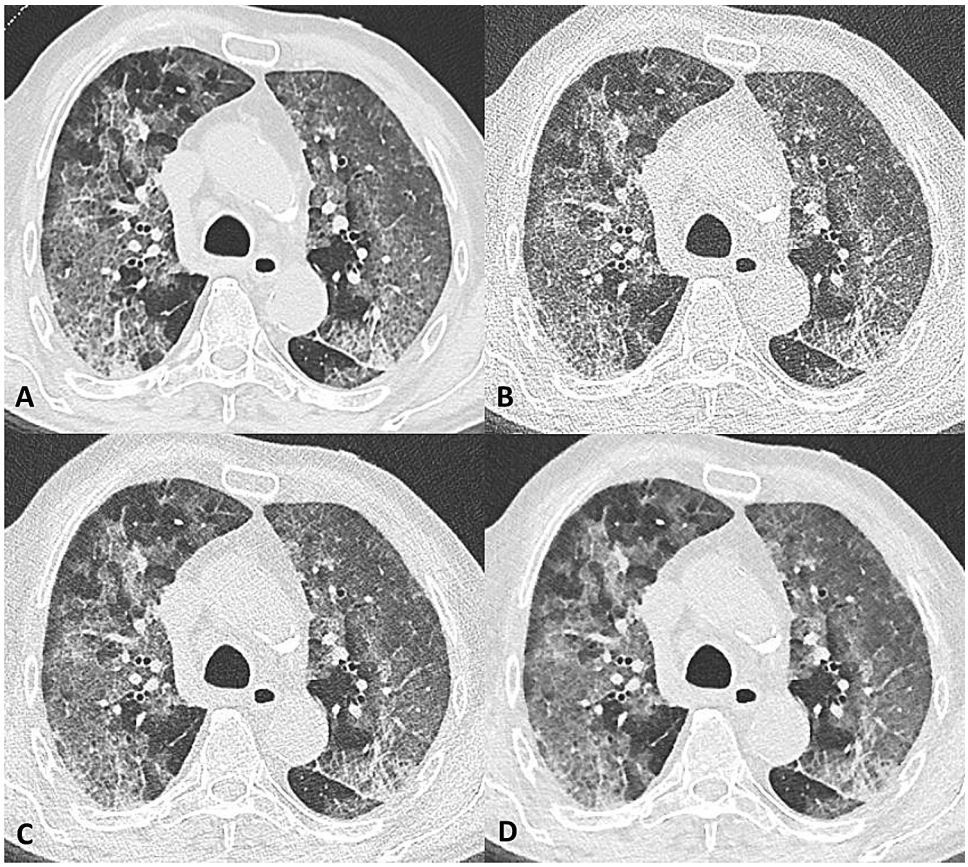

Fig. 6 Extended ground glass opacities with superimposed septal thickening in a 89-year-old male patient with BMI of 28. **a** Dual-energy CT, 90/150Sn kV, ADMIRE 3. **b** High-pitch, dual-source acquisition with spectral shaping at 100 kV, filtered backprojection (LDCT0). **c** High-pitch, dual-source acquisition with spectral shaping at 100 kV, ADMIRE 3 (LDCT3). **d** High-pitch, dual-source acquisition with spectral shaping at 100 kV, ADMIRE 5 (LDCT5). In A (DECT3), the septal thickening is clearly visible in both upper lobes. In LDCT (**b**, **d**), the septal thickening is better outlined with ADMIRE (**c**, **d**); however, with ADMIRE 5 (**d**) the smoother texture of the image hides the septal thickening which is visible with ADMIRE 3 (**c**)

recognition tasks became more challenging (Table 3, Fig. 6). The added value of these data is in the evaluation of low-contrast recognition tasks on a high-pitch, dual-source CT protocol: most of the available evidences evaluated the dual-source acquisitions with or without spectral shaping in pediatric populations; conversely, in adults, the high-pitch, dual-source acquisitions are not fully standardized for pulmonary imaging and the assessed protocols with spectral shaping include single-source acquisitions at standard pitch values [12–17].

This study has some limitations. It is a single-center study in a relatively small population. The present work evaluates a single CT technology: in this pandemic setting, a specific CT scanner in a separate wing of the Department of Radiology was reserved for the baseline examinations of COVID-19 hospitalized patients. Moreover, even though the image was anonymized, the readers might have recognized them because their different appearance and texture with potential recognition bias. Finally, to maintain a homogeneous sample, different blending rations of DECT3 were not included in the analysis.

In conclusion, the low-dose, dual-source CT protocol with spectral shaping is feasible and effective in the management of motion artifacts in symptomatic patients with COVID-19 pneumonia, with significant dose reduction, valuable in repeated examinations. The ADMIRE was fundamental in the optimization of the low-dose protocol, even in overweight patients, without significant improvement of the low-contrast recognition tasks at higher strengths, suggesting intermediate strengths as optimal.

Compliance with ethical standards

Conflict of interest A.A. is a speaker for Siemens Helthineers. The other authors declare that they have no conflict of interests.

Ethical standards All procedures in studies involving human participants were in accordance with the ethical standards of the institutional and/or national research committee and with the 1964 Declaration of Helsinki and its later amendments or comparable ethical standards.

References

1. John Hopkins University (2020) COVID-19 Dashboard by the Center for Systems Science and Engineering (CSSE) at Johns Hopkins University (JHU). Available via https://coronavirus.jhu.edu/map.html. Accessed 25 Aug 2020
2. Rubin GD, Ryerson CJ, Haramati LB et al (2020) The role of chest imaging in patient management during the COVID-19 pandemic:

a multinational consensus statement from the fleischner society. Radiology 0:201365
3. Yuki K, Fujiogi M, Koutsogiannaki S (2020) COVID-19 pathophysiology: a review. Clin Immunol. https://doi.org/10.1016/j.clim.2020.108427:108427
4. Ye Z, Zhang Y, Wang Y, Huang Z, Song B (2020) Chest CT manifestations of new coronavirus disease 2019 (COVID-19): a pictorial review. Eur Radiol. https://doi.org/10.1007/s00330-020-06801-0
5. Caruso D, Zerunian M, Polici M et al (2020) Chest CT features of COVID-19 in Rome, Italy. Radiology. https://doi.org/10.1148/radiol.2020201237:201237
6. Pan F, Ye T, Sun P et al (2020) Time course of lung changes on chest CT during recovery from 2019 novel coronavirus (COVID-19) pneumonia. Radiology. https://doi.org/10.1148/radiol.2020200370:200370
7. Wang Y, Dong C, Hu Y et al (2020) Temporal changes of CT findings in 90 patients with COVID-19 pneumonia: a longitudinal study. Radiology. https://doi.org/10.1148/radiol.2020200843:200843
8. Tabatabaei SMH, Talari H, Moghaddas F, Rajebi H (2020) Computed tomographic features and short-term prognosis of coronavirus disease 2019 (COVID-19) pneumonia: a single-center study from Kashan, Iran. Radiol: Cardiothoracic Imaging 2:e200130
9. Sakane H, Ishida M, Shi L et al (2020) Biological effects of low-dose chest CT on chromosomal DNA. Radiology 0:190389
10. Kang Z, Li X, Zhou S (2020) Recommendation of low-dose CT in the detection and management of COVID-2019. Eur Radiol. https://doi.org/10.1007/s00330-020-06809-6
11. Lell MM, Scharf M, Eller A et al (2016) Feasibility of respiratory-gated high-pitch spiral CT. Acad Radiol 23:406–412
12. Gordic S, Morsbach F, Schmidt B et al (2014) Ultralow-dose chest computed tomography for pulmonary nodule detection: first performance evaluation of single energy scanning with spectral shaping. Invest Radiol 49:465–473
13. Haubenreisser H, Meyer M, Sudarski S, Allmendinger T, Schoenberg SO, Henzler T (2015) Unenhanced third-generation dual-source chest CT using a tin filter for spectral shaping at 100kVp. Eur J Radiol 84:1608–1613
14. Martini K, Higashigaito K, Barth BK, Baumueller S, Alkadhi H, Frauenfelder T (2015) Ultralow-dose CT with tin filtration for detection of solid and sub solid pulmonary nodules: a phantom study. Br J Radiol 88:20150389
15. Martini K, Barth BK, Nguyen-Kim TDL, Baumueller S, Alkadhi H, Frauenfelder T (2016) Evaluation of pulmonary nodules and infection on chest CT with radiation dose equivalent to chest radiography: prospective intra-individual comparison study to standard dose CT. Eur J Radiol 85:360–365
16. Xu X, Sui X, Song L et al (2019) Feasibility of low-dose CT with spectral shaping and third-generation iterative reconstruction in evaluating interstitial lung diseases associated with connective tissue disease: an intra-individual comparison study. Eur Radiol 29:4529–4537
17. Weis M, Henzler T, Nance JW Jr et al (2017) Radiation dose comparison between 70 kVp and 100 kVp with spectral beam shaping for non-contrast-enhanced pediatric chest computed tomography: a prospective randomized controlled study. Invest Radiol 52:155–162
18. Agostini A, Floridi C, Borgheresi A et al (2020) Proposal of a low-dose, long-pitch, dual-source chest CT protocol on third-generation dual-source CT using a tin filter for spectral shaping at 100 kVp for CoronaVirus Disease 2019 (COVID-19) patients: a feasibility study. La Radiol Medica. https://doi.org/10.1007/s11547-020-01179-x
19. Hansell DM, Bankier AA, MacMahon H, McLoud TC, Müller NL, Remy J (2008) Fleischner society: glossary of terms for thoracic imaging. Radiology 246:697–722
20. Chang YC, Yu CJ, Chang SC et al (2005) Pulmonary sequelae in convalescent patients after severe acute respiratory syndrome: evaluation with thin-section CT. Radiology 236:1067–1075
21. Mettler FA Jr, Huda W, Yoshizumi TT, Mahesh M (2008) Effective doses in radiology and diagnostic nuclear medicine: a catalog. Radiology 248:254–263
22. Albarello F, Pianura E, Di Stefano F et al (2020) 2019-novel Coronavirus severe adult respiratory distress syndrome in two cases in Italy: an uncommon radiological presentation. International Journal of Infectious Diseases 93:192–197
23. Chung M, Bernheim A, Mei X et al (2020) CT imaging features of 2019 novel coronavirus (2019-nCoV). Radiology 295:202–207
24. Brown K, Mund DF, Aberle DR, Batra P, Young DA (1994) Intrathoracic calcifications: radiographic features and differential diagnoses. RadioGraphics 14:1247–1261
25. Jones EL, Cameron AH (1969) Pulmonary calcification in viral pneumonia. J Clin Pathol 22:361–366
26. Watzke O, Kalender WA (2004) A pragmatic approach to metal artifact reduction in CT: merging of metal artifact reduced images. Eur Radiol 14:849–856
27. Baker ME, Dong F, Primak A et al (2012) Contrast-to-noise ratio and low-contrast object resolution on full- and low-dose MDCT: SAFIRE versus filtered back projection in a low-contrast object phantom and in the liver. AJR Am J Roentgenol 199:8–18
28. Jensen CT, Wagner-Bartak NA, Vu LN et al (2019) Detection of colorectal hepatic metastases is superior at standard radiation dose CT versus reduced dose CT. Radiology 290:400–409
29. Shaqdan KW, Kambadakone AR, Hahn P, Sahani DV (2018) Experience with iterative reconstruction techniques for abdominopelvic computed tomography in morbidly and super obese patients. J Comput Assist Tomogr 42:124–132
30. Yu L, Vrieze TJ, Leng S, Fletcher JG, McCollough CH (2015) Technical note: measuring contrast- and noise-dependent spatial resolution of an iterative reconstruction method in CT using ensemble averaging. Med Phys 42:2261–2267